Properties of Single Oxygen Vacancies on a Realistic $(TiO_2)_{84}$ Nanoparticle: A Challenge for Density Functionals

Ángel Morales-García, Oriol Lamiel-García, Rosendo Valero, Francesc Illas*

Departament de Ciència de Materials i Química Física & Institut de Química Teórica i Computacional (IQTCUB), Universitat de Barcelona,
c/ Martí i Franquès 1, 08028, Barcelona, Spain.

Abstract

Based on all electron relativistic density functional theory (DFT) calculations, the properties of single oxygen vacancies in TiO_2 nanoparticles have been obtained using a suitable representative model consisting of an octahedral $(TiO_2)_{84}$ nanoparticle of ~3 nm size terminated with (101) facets. This nanoparticle can be safely considered at the onset of the so-called scalable regime where properties scale linearly with size towards bulk like limit and hence results can be more directly compared to experiment. A set of reduced $Ti_{84}O_{167}$ nanoparticles are selected to investigate the geometrical, energetical and electronical properties by using PBE semi-local functional with three different amounts of Fock exchange 0% (PBE), 12.5% (PBEx) and 25% (PBE0). In particular, using the PBEx hybrid functional, previously validated for bulk anatase and rutile, it is predicted that the highly (three)-coordinated oxygen atom, located in the subsurface, and the least coordinated one at top sites are energetically the most suitable candidate for generating the oxygen vacancy. The subsurface case is in line with conclusions from experiments carried out on (101) single crystal anatase surfaces. The electronic structure of the reduced particles suggests that these would have better photocatalytic activity than their stoichiometric counterparts. Nevertheless, several properties of reduced TiO_2 NPs are strongly affected by the choice of the exchange-correlation functional implying that, in absence of validation by comparison to experiment, predictions must be taken with caution

Introduction

Titanium dioxide (TiO_2), a semiconducting metal oxide, is widely used as a photocatalyst because of its chemical stability, low cost, and nontoxicity.[1-4] Both rutile and, especially, anatase nanostructures catalyze the overall splitting of water into molecular hydrogen and oxygen when illuminated with ultraviolet (UV) light.[5-8] This photocatalytic process represents a promising clean and sustainable alternative to fossil fuels.[9,10] However, applications of TiO_2 show a low quantum yield (QY) and limited harvesting of visible light which is a direct consequence of the too large band gap of this material. Moreover, fast recombination of photogenerated electron-hole pairs represents an additional problem. To tackle the above obstacles, several strategies have been applied to modify TiO_2, like depositing noble metals (e.g. Pt),[11] doping with transition-metal ions (e.g. Cu) or nonmetal elements (e.g. N),[12] adding electron carriers (e.g. graphene)[13] or coupling to small band gap quantum dots (e.g. PdS).[14] In addition, TiO_2 nanostructuring with specific morphologies and crystal facets has emerged as a promising way to improve the QY with visible light.[15,16]

Alternatively, engineering defects on the TiO_2 nanostructures appears as another encouraging way to circumvent the aforementioned low QY of TiO_2.[17] It has been reported that creating a highly disordered surface layer and a large amount of oxygen vacancies (O_v) in TiO_2 not only improves visible and near-infrared light absorption but also leads to a superior activity in photocatalytic degradation of organic pollutants and H_2 evolution from H_2O.[18] From simple electron counting and assuming formal oxidation states, one neutral oxygen vacancy, O_v, provides two excess electrons to the TiO_2 system, and these electrons are available for the reduction of Ti^{4+} to Ti^{3+}. Indeed, the formation of Ti^{3+} center has been confirmed by experiments such as photoelectron spectroscopy and electron paramagnetic resonance (EPR).[19,20] Recently, it has been shown that Ti^{3+} self-doped TiO_2 nanocrystals with a 1:80 Ti^{3+}:Ti^{4+} ratio exhibit a remarkable enhancement of the photocatalytic efficiency; this is precisely ascribed to the presence of Ti^{3+} centers and concomitant O_v point defects.[21] The combination of O_v and Ti^{3+} centers leads to specific electronic structure features usually referred to as trapped electrons. These states appear around 1.0 eV below the conduction band minimum (CBM), which induces band gap narrowing. Engineering Ti^{3+}/O_v sites can favorably promote CO_2 activation and conversion to CO under visible light.[22] Several computational studies have focused on these systems and reported the properties of O_v in bulk, surface and subsurface TiO_2 sites.[23-25] Experiments and calculations show that formation energy of neutral oxygen vacancy is lower when defect site is located in the subsurface of anatase (101) and (001) surfaces, whereas the surface site is the most stable site in rutile (110) surface. Similar

information on TiO_2 nanostructures is so far lacking except for a recent study on a $(TiO_2)_{35}$ representation of an octahedral nanoparticle.[26] This is indeed the smallest TiO_2 NP compatible with Wulff construction, yet metastable with respect to non-crystalline structures[27] as further commented below.

The electronic properties of TiO_2 nanoparticles (NPs) have been discussed in the light of experiments reporting that the control of the shape and size of titania NPs modulates the photoactivity.[15] The understanding of TiO_2 NP properties is particularly attractive because its size and shape are appropriate to rationalize the experimental evidences.[28] However, experimentally, it is difficult to discern between the different effects of size and shape and those introduced by the synthetic conditions. The difficulties encountered by experiments to separate complex factors are not present when employing computational models in which one can represent different morphologies for a given composition or vary the composition for a given morphology.[27,29-31] For instance, the analysis of the atomic structure of TiO_2 small clusters and NPs of increasing size allows one to estimate the dimensions for emergence of crystallinity and scrutiny of electronic properties of well defined nanoparticles allows one to identify the size-limit of titania NP at which the properties show an asymptotic trend towards bulk-like behavior.[30] In particular, it has been shown that the realistic $(TiO_2)_{84}$ anatase NP is at the start of the scalable regime limit above which properties of titania NPs scale linearly towards bulk limit values. Assuming spherical shape[32] one would get an estimate size of 3 nm for the octahedral $(TiO_2)_{84}$ NP, a value which nicely fits with the predicted height from a linear relationship between the largest vertex to vertex distance in octahedral TiO_2 NPs and the cubic root of the number of TiO_2 units.[30] From both arguments one can conclude that $(TiO_2)_{84}$ anatase NP is an appropriate model system to investigate the changes induced by the generation of O_v in their electronical and structural properties and hence in its photocatalytic activity.

Herein, using state of the art density functional theory (DFT) based methods, we systematically investigate the properties of oxygen vacancies in an initially stoichiometric $(TiO_2)_{84}$ anatase NP. To facilitate the study and handle the numerous possible isomers resulting from the creation of a single O_v in this quite large NP, we follow the strategy developed in a preliminary study on a smaller $(TiO_2)_{35}$ anatase NP.[26] We have already mentioned that this is the smallest size for a bulk cut octahedral NP exhibiting (101) facets although in terms of total energy per TiO_2 unit it is clearly metastable.[27] This fact can affect the conclusions regarding reduction and ask for subsequent studies on a more realistic model. This is precisely the main reason to undertake the present work on the properties of oxygen vacancies on the $(TiO_2)_{84}$ NP. Several possible sites for

oxygen vacancy formation are evaluated according to the position and the coordination number (CN), using results for oxygen vacancy in $(TiO_2)_{35}$ as a convenient guide.[26]

Computational Details

First of all, it must be recalled that standard density functionals within the Generalized Gradient Approach (GGA) fail to provide even a qualitatively correct description of electronic properties in stoichiometric and reduced TiO_2 systems due to an exceedingly large effect of the so-called self-interaction error inherent to the Kohn-Sham practical implementation of DFT.[33,34] To correctly describe the partial occupation and appropriate localization of states arising from Ti^{3+} sites hybrid functionals are required where a given percent of Fock exchange is mixed into a given exchange GGA functional. Assuming that the Kohn-Sham energy levels provide an estimate of the binding energies of quasiparticles, previous studies have shown that modifying the PBE0 (25% Fock)[35,36] functional so as to contain 12.5% of Fock exchange (PBEx) reproduces successfully experimental band gap of anatase and rutile polymorphs whereas the commonly used PBE0 hybrid functional[35] significantly overestimates them.[23] In addition, PBEx functional describes properly the properties of the O_v in both rutile and anatase TiO_2 bulk phases.[23]

In the present study DFT based calculations have been carried with the PBEx hybrid functionals. However, in the view of the strong influence of the exchange-correlation functional on the outcome of the calculation, results from more traditional approaches such as PBE[36] and PBE0[35] are included for comparison. Another aspect regarding the accuracy of the density functional methods chosen concerns the contribution of dispersion terms. For the atomic structure of bulk anatase and rutile, Deringer and Scányi[37] found rather small changes in the predicted lattice parameters when taking into account these effects on top of results obtained from PBE. The changes are similar those encountered when going from PBE to PBEx. Consequently, the contribution of dispersion has not been further considered.

All calculations explicitly include all electrons and the electron density is described through a numerical atom-centered (NAO) orbital basis set, as implemented in the Fritz Haber Institute *ab initio* molecular simulations (FHI-aims) package.[38] The light grid and tier-1 basis set are selected, the numerical accuracy of this basis set for TiO_2 systems is similar to that of a valence triple-ζ plus polarization Gaussian type orbitals (GTO) basis.[30] Recent studies have further assessed the quality of the light tier-1 NAO basis set on the stability and electronic properties of TiO_2 NPs.[31] The convergence threshold for atomic forces in relaxation of pristine and reduced $(TiO_2)_{84}$ NPs is set to 10^{-2} eV $Å^{-1}$. The presence of a transition element like Ti requires the inclusion of relativistic effects

to properly ensure sufficient accuracy for calculated properties. In the present work, relativistic effects are included through the zero order regular approximation (ZORA).[39,40]

A series of reduced $Ti_{84}O_{167}$ NPs has been considered which differ in the position where the oxygen vacancy has been created. The considered NPs have all formally two Ti^{3+} centers and hence involve two excess electrons leading to different electronic states— closed shell singlet, open shell singlet and triplet— depending on the spin coupling. Hereby, closed-shell singlet and open-shell triplet states are considered as in previous work.[26] The oxygen vacancy formation energy, E_f^O, is calculated as:

$$E_f^O = E(Ti_{84}O_{167}) + \frac{1}{2}E(O_2) - E(Ti_{84}O_{168}) \qquad (1)$$

where. $E(O_2)$ stands for the energy of O_2 molecule in its triplet ground state and $E(Ti_{84}O_{167})$ and $E(Ti_{84}O_{168})$ correspond to the total energies of a given reduced $Ti_{84}O_{167}$ NP and of the pristine $(TiO_2)_{84}$ one. In all cases, the structure of the NP is fully relaxed for each one of the functionals employed in this study. According to definition of Eq. (1), a positive value of E_f^O is associated with the extra energy required for removing a neutral single oxygen. We also define the vertical energy (E_v) which is calculated as in Eq. (1) but using the energy of the non-relaxed reduced $Ti_{84}O_{167}$ NP and the relaxation energy (E_{rel}) defined as $E_{rel} = E_v - E_f^O$. Further details about the definition of energies are schematically given in Supporting Information.

Results and Discussion

It is necessary to insist on the fact that the contribution of non-local, exact, Fock exchange to the exchange-correlation potential has a marked influence in predicted properties of oxides in general and of TiO_2 related systems, in particular. Precisely, this is an especially delicate issue for the properties of O_v containing systems exhibiting unpaired electrons strongly localized at Ti^{3+} centers but with the degree of localization depending on the choice of the exchange-correlation potential. To rigorously tackle this problem and to avoid any particular bias, this section is divided into two parts. In the first one, properties of O_v on reduced $Ti_{84}O_{167}$ NPs are discussed in light of results obtained with the PBEx functional which, as pointed out above, properly describes stoichiometric and reduced bulk TiO_2. In the second part the influence of the Fock exchange contribution in the exchange-correlation potential is analyzed in some details so as to reach unbiased conclusions regarding the interpretation on vacancy defect states in the $Ti_{84}O_{167}$ NPs. To this end, results have been obtained from the PBE and PBE0 functionals. Results from the later are explicitly discussed here whereas the former are reported in the Supporting Information.

Properties of $O_v@Ti_{84}O_{168}$ *as described from the PBEx functional*

The optimized structure of the realistic $(TiO_2)_{84}$ NP obtained from a Wulff construction[41,42] and featuring the most stable (101) facets[43] is shown in Figure 1. To systematically examine the effect of a single oxygen vacancy one would need to consider all possibilities which, even exploiting symmetry, faces a combinatorial explosion. Therefore, we rely on results obtained from an earlier systematic study on the smaller $(TiO_2)_{35}$ NP[26] and choose the most favorable sites for O_v as candidates for $(TiO_2)_{84}$ NP. This is justified because both NPs have the same octahedral shape, symmetry and exposed (101) facets.[26,28] Figure 1 displays the fully optimized atomic structure of the stoichiometric $(TiO_2)_{84}$ and of different reduced $Ti_{84}O_{167}$ NPs that are obtained after removal of a selected single oxygen atom. The vacancy sites considered are classified according to the following notation: top (T), edge (E), facet (F), and inside (I) types which clearly define the position of the removed oxygen. To further identify each single O vacancy, we use the X-m notation where X and *m* designate domain type (T, E, F or I) and CN (1, 2 or 3) respectively. For instance, F-3 corresponds to the removing an oxygen atom coordinated to three Ti atoms (CN = 3) in the facet (F) domain. Note also that an additional digit (1 or 2) is used to distinguish two I-3 analog sites.

We start analyzing two different optimized structures of the pristine $(TiO_2)_{84}$ NP, which just depend on the orientation of apical oxygen atoms: (*i*) almost linear, straight tip, or (*ii*) bent to opposite sides, bent tip (see Figure 3 in Ref. [30]). The bent tip structure depicted in Fig. 1a is energetically more stable by around 0.011 eV per TiO_2 unit (0.96 eV in absolute terms) for all employed DFT functionals, consistent with the previous analysis over $(TiO_2)_{35}$ NP where a similar favorable energetic stability for bent tip structure was found (1.06 eV in absolute terms).[26] We assume that the difference between straight and bent tip structures tends to be negligible by increasing the size of TiO_2 NP although this is not an important issue. In fact, despite their slight structural difference, the electronic band gap (E_{gap}), evaluated as the difference between the highest occupied molecular orbital (HOMO) and the lowest unoccupied molecular orbital (LUMO) is almost the same. This value, however, strongly depends on the exchange-correlation potential used to describe the electronic structure and PBEx functional nicely reproduces[23] the experimental E_{gap} of 3.20 eV of bulk anatase phase.[44] For the stoichiometric $(TiO_2)_{84}$ NP, the PBEx functional calculated E_{gap} is 3.49 and 3.61 eV for straight and bent tip structures, respectively. Here, it is noted that for small nanoparticles E_{gap} depends significantly on the geometrical structure[29] although the effect fades away for larger particles in the scalable regime.[30]

To avoid any possible artifacts, the properties of O_v in $(TiO_2)_{84}$ NP are studied by removal of one neutral oxygen atom from the bent tip structure (Figure 1). Six oxygen sites are selected and

systematically removed one at a time. This set of $Ti_{84}O_{167}$ reduced nanoparticles represents the structures that have the lowest E_f^O in each one of the domains based on our previous study of $(TiO_2)_{35}$ NP[26] having the same morphology and exhibing the same facets as commented above. Table 1 reports the values of E_v, E_{rel}, E_f^O and the energy level of the oxygen vacancy defect state below LUMO (S_v-1 and S_v-2) calculated at the PBEx level. Note that the oxygen vacancy sites with just a S_v-1 energy correspond to a closed-shell singlet state which is found to be the electronic ground state after geometry optimization. This is quite an unexpected result since spin polarized solutions are the ground state for O_v in bulk anatase and comes from the differences in structural relaxation that are possible in the NP as compared to the bulk or extended surfaces. In fact, the rather broad range of E_f^O values for the different sites appears to be due to differences in the structural relaxation of the reduced $Ti_{84}O_{167}$ NPs. The vacancy formation is largely determined by the structural features around the oxygen vacancy site. For the PBEx functional, E_f^O appears in the 3.56–4.27 eV range, a prediction fully consistent with those previously reported using the same PBEx functional for anatase bulk phase, with E_f^O values in the 4.21–4.65 eV range, and for the $(TiO_2)_{35}$ NP, although in this case E_f^O involves a broader range (2.27–5.15 eV).[23,26]

Figure 2 displays trends for E_f^O in the $Ti_{84}O_{167}$ nanoparticle, I-3-2 site has the lowest E_f^O value of 3.56 eV (see Table 1). Note, however, that the T-1 domain is energetically competitive showing an energy difference of 0.02 eV only. Another highlighted energetic parameter is the vertical energy E_v (Table 1). It is observed that O_v formation at I-3-2 site features the lowest vertical energy value (4.29 eV) whereas the largest one (5.26 eV) corresponds to the formation of the unrelaxed O_v at F-2 site. On the other hand, for the I-3-2 and F-2 site, E_{rel} values of ~0.72 and ~1.31 eV, respectively are obtained. Note that, except for the F-2 site, E_{rel} varies in a narrow range of 0.7–0.9 eV so that, within 0.2 eV, the stability of the different possible single oxygen vacancies is hence dominated by the E_v energy. This energetic analysis confirms that the O_v formation is preferentially located inside the nanoparticle in the subsurface region instead of directly at surface terraces.

According to experimental evidences, surface oxygen vacancies are not present on freshly cleaved anatase (101) samples.[45,46] A reduced anatase (101) crystal shows isolated as well as ordered intrinsic subsurface defects in scanning tunneling microscopy (STM), consistent with DFT calculations for surface slab models which predict that O_v at subsurface and bulk sites are significantly more stable than on the surface.[45,46] Note that O_v at T-1 site is essentially as stable as at I-3-2 site but, it is a feature that (*i*) is not present in extended crystalline (101) anatase surfaces and (*ii*) unique to the morphology of the nanoparticle, thus it would not be found in extended surfaces.

The prediction from the present all electron relativistic DFT based calculations for realistic TiO_2 NP are in agreement with the experimental evidence and provides further support to the claim that $(TiO_2)_{84}$ corresponds to a particle size in the scalable regime and hence representative of the large NPs used in the experiments. This provides additional support to the choice of the PBEx hybrid functional as appropriate to investigate the properties of stoichiometric and reduced realistic TiO_2 NP as suggested from previous studies.[23,26,31]

We discuss now in some detail the structural changes around the first neighbor titanium atoms to each of the investigated O_v sites (Figure 3). The reorganization of the structure around the vacant space and the presence of the Ti^{3+} sites arising from the two excess electrons are the major factors in the relaxation of the reduced $Ti_{84}O_{167}$ NPs. To understand the quantitative analysis of E_f^O (Table 1), we carefully analyze the geometrical differences between pristine and reduced $(TiO_2)_{84}$ anatase NPs for each one of the O_v. Oxygen vacancy at the T-1 and I-3-2 sites show the lowest E_f^O, 3.56 and 3.58 eV respectively, that is consistent with the negligible variation of Ti-O distance once the oxygen vacancy is created (Figures 3a, 3e). Contrarily, O_v at the I-3-1 site (Figure 1a) shows noticeable structural changes requiring 0.47 eV more than the O_v at the I-3-2 site although this energy difference is already present in the values of E_v. Accordingly, this extra energy requirement cannot be attributed to the noted changes in the structural properties (Figure 3a). Assuming these arguments, the most favorable domains to accommodate O_v are mainly dictated by the initial structure with the atomic reorganization around the vacant space playing a minor role. Considering both effects, the ranking of site for O_v ordered from the lowest to the highest oxygen formation energy is I-3-2 ~ T-1 < F-2 < E-2 < I-3-1 < F-3.

Finally, we consider the effect of the presence of Ti^{3+} ions in reduced TiO_2 NP in the resulting electronic structure. The existence of Ti^{3+} can be regarded as one type of n-type doping of TiO_2 samples. From a theoretical point of view, the description of Ti^{3+} centers in TiO_2 systems is not straightforward since PBE predicts physically meaningless fully delocalized whereas hybrid functionals predict a variety of near degenerate solutions with different degrees of localization as described in the literature.[47] Nevertheless, upon O_v formation a band gap narrowing is observed in all cases.[19,21,26] In bulk samples, experiments show that the defect state appears at around 1 eV below CBM, a feature which is reproduced by the PBEx functional.[22] Figure 4 presents the PBEx molecular orbital energy level diagram of $Ti_{84}O_{167}$ NP for a total of six O_v sites . Note that here all energy (quasi band) levels are referenced with respect to the vacuum.[48] The defect states are reported as singly (triplet state) or doubly (singlet state) occupied molecular orbitals. Only spin-up eigenvalues are shown because molecular energy levels of spin-up and spin-down singlet and triplet

states are similar. The spin-unrestricted triplet state is competitive with the closed-shell singlet one in reduced TiO_2 NPs, a feature which is specific of the reduced NPs and does not appear in the bulk anatase. It is clearly shown that the defect states appear between HOMO and LUMO and that, not surprisingly, the E_{gap} and S_v values vary with O_v site. The presence of the O_v defect also affects the position of the HOMO and LUMO energy levels so that new electronic transitions both from HOMO and defect states to LUMO and from HOMO to defect states become possible.

Effect of the amount of Fock exchange on the Properties of $O_v@Ti_{84}O_{168}$

We discuss now in detail the effect of percentage of Fock contribution on vacancy defect states comparing PBEx and PBE0 results. The pure GGA type PBE functional has also been considered for completeness although given the shortcomings of this approach in describing the electronic structure of oxides, the corresponding results are reported in the Supporting Information.

We start by describing the effect of the functional on the calculated values of E_v, E_{rel} and E_f^O . The contribution of Fock exchange has a relatively low influence on E_v as one can readily see by comparing PBEx and PBE0 results in Tables 1 and 2. The largest E_v difference between these two hybrid functionals is of 0.7 eV and corresponds to the F-3 and I-3-2 domains. On the other hand, significantly larger differences are encountered for E_{rel} ranging now between 2.44 and 3.34 eV which make the E_f^O values calculated by the PBE0 functional significantly smaller than those obtained from calculations using PBEx functional. The fact that PBE0 functional with a larger (25%) contribution of the Fock exchange involves a larger contribution to the energy gain upon relaxation of the reduced $Ti_{64}O_{167}$ NP is consistent with a larger degree of localization of trapped electrons in the Ti^{3+} centers with a concomitant larger structural relaxation; for instance, the F-3 domain increases in 0.7 and 2.18 eV for E_v and E_{rel}, respectively. This is indeed the main energetic term that leads to E_f^O below 3.0 eV (see Figure 2 and Table 2). Although PBE0 calculated E_f^O values are smaller than those predicted from PBEx, the stability of the different possible single oxygen vacancies continues to be governed by the E_v quantity following the same argument explained at PBEx level earlier. The PBE0 calculations predict that the most preferential site to form the O_v is located at tip (T-1) and facet domain (F-2). The T-1 case is not so surprising as this is also the preferred site for O_v in ceria nanoparticles,[49,50] the larger localization induces a larger relaxation and the final result is perhaps as expected, the lowest coordinated O atom is the easiest to remove. This is also in agreement with the results obtained with the PBEx functionals which predicts that O_v is almost equally favorable at T-1 and I-3-2 sites. The F-2 case is harder to understand and it is not consistent with the experimental findings for extended surfaces perhaps due

to its proximity to the nanoparticle edge (see Figure 1).[45,46] In any case, it is important to point out that the differences in E_f^O for the different most stable sites are of the order of 0.3 eV only and this is perhaps in the error bar of this type of DFT based calculations for this property. Nevertheless, the final E_f^O calculated values are much smaller with PBE0 functional implying that TiO_2 appears to be more reducible than predicted with PBEx. Unfortunately, without a guide from experiment it is hard to assess which of the two functionals better describes TiO_2 reduced nanoparticles and, in the view of the better performance of PBEx functional for stoichiometric and reduced rutile and anatase one is tempted to suggest that this will be also the case for the reduced NPs even if some feature is counterintuitive.

Although the experimental indications are not completely corresponding with predictions from the PBE0 functional, this approach reproduces the degree of localization on the neighboring Ti atoms, which are reduced to Ti^{3+} in the I-3-2 site, which is not always observed by using PBEx functional (see Figure 4). Note that whereas PBEx functional gives the most favorable site at I-3-2 site consistent with the experiments for extended anatase (101) surfaces, it does not appropriately reproduce the oxygen vacancy defect state below LUMO (Figure 4) promoting a doubly (singlet state) occupied molecular orbital. This issue is solved when the percentage of Fock contribution increases (PBE0 functional) giving singly (triplet state) occupied molecular orbitals as shown in Figure 5.

Therefore, one must conclude that the appropriate selection of the exchange-correlation functional to investigate the properties of reduced TiO_2 NPs requires a thorough examination of a range of properties and to analyze how the amount of Fock exchange affects them. In the case of O_v in TiO_2 NPs there is a certain degree of incertitude on determining exactly the most stable one although one can for sure make more reliable predictions by focusing on a range of formation energies including various possibilities. This is supported by analysis of Figure 2 clearly showing that PBEx and PBE0 functionals exhibit similar trends regarding the energy formation of different O_v and that this is clearly different from the trend predicted by PBE functional. Also, describing properly the stability and the electronic structure of O_v related states is far from being a solved problem since the amount of Fock exchange required to accurately describe the gap is insufficient to produce the expected localization. The latter remains, nevertheless, to be confirmed by experiments on suitable nanoparticles.

Conclusions

The properties of neutral single oxygen vacancy in realistic anatase nanoparticles have been investigated by choosing a suitable model and making use of all electron relativistic DFT based calculations within the PBEx hybrid functional previously optimized to reproduce the structure and electronic properties of bulk, stoichiometric and reduced, anatase and rutile.[23] The model chosen is a $(TiO_2)_{84}$ anatase nanoparticle of ~3 nm size terminated with (101) facets which is at the onset of scalable regime and a total of six different sites have been systematically investigated to analyze the structural and electronic properties of various isomers of the reduced $Ti_{84}O_{167}$ nanoparticle.

The oxygen vacancy formation and the energy levels of the defect state are quite dependent on the site from which the oxygen atom is removed. From energy arguments, the most favorable oxygen vacancy is the three-coordinated domain located at the subsurface region, being in nice accordance with experimental evidences observed in anatase well defined surfaces.[45,46] The latter is an additional argument in support of the claim that this particle size is well in the scalable regime and can be taken as representative of larger nanoparticles for future studies involving for instance hydroxylation and/or doping. Nevertheless, the formation of a vacancy produced by removing the least coordinated O atom is almost as favorable and becomes the most favorable one according to calculations with the PBE0 functional.

The present calculations predict a HOMO-LUMO gap for the pristine nanoparticle of 3.61 eV and the presence of defect states in the reduced nanoparticle in the 0.49–1.68 eV range below the LUMO energy level, which are mostly due to the presence of Ti^{3+} cations. In some cases, the PBEx electronic ground state of the reduced nanoparticles appears to be a closed singlet, even optimizing structures with atomic displacements around O_V (see I-3-2 site in Figures 3 and 4) which is at variance with the behavior found for bulk anatase and its extended surfaces. Here, PBE0 functional predicts that the electronic ground state is a triplet with two singly occupied orbitals located in two Ti^{3+} cations more in line with expectations from chemical intuition and with experiments in bulk and extended surfaces. Therefore, although we rely mostly on the conclusions based on the results obtained from calculations with the PBEx hybrid functional, one must admit that the influence of the functional is large and, in some cases, the site predicted to lead to the most stable reduced nanoparticle and the character of the oxygen vacancy containing nanoparticles electronic ground state can vary with the amount of Fock. The fact that PBEx functional reproduces most of the quantities related to stoichiometric and reduced anatase and rutile provides support to the present conclusions for the reduced nanoparticles but also points out that the choice of the DFT based method is far from being a settled problem. The positive part is, however, that many

qualitative trends are less dependent on the functional. The overall reduction of the band gap of the reduced nanoparticle together with the presence of defect states suggest that reduced nanoparticles would be better suited to harvest light in the visible. However, the standard redox analysis does not clearly confirm that reduced TiO_{2-x} NPs can be applied to visible light absorbing photocatalyst for the water splitting photocatalytic process.

Although the realistic TiO_2 NP studied here seems appropriate to unravel the features of reduced nanoparticles, further studies are required to shed light on the photoreactivity of reduced TiO_2 NPs towards water splitting considering for instance multi-oxygen vacancy effects, migration of oxygen vacancies and solvation effects. Note that the present study may be extended to investigate reduced photocatalysts which show ability to directly utilize solar energy for producing solar fuels such as H_2, CH_4 or CH_3OH.[51]

ASSOCIATED CONTENT

Supporting Information

The Supporting Information is available free of charge on the ACS Publications website at DOI:

The description of energetic scheme is shown in Figure S1. Oxygen vacancy formation energies, Kohn-Sham orbital energy level diagrams and structural properties are described in Table S1 and Figures S2 and S3 for PBE level. Whereas, structural properties at PBE0 level are depicted at Figure S4.

AUTHOR INFORMATION

Corresponding Author

* E-mail: francesc.illas@ub.edu

Notes

The authors declare no competing financial interest.

ACKNOWLEDGEMENTS

The authors are indebted to Prof. Ulrike Diebold for pointing out the similarity of the present results to those measured in her group for anatase TiO_2 (101) surfaces. This research was supported by the Spanish MINECO/FEDER CTQ2015-64618-R grant and, in part, by Generalitat de Catalunya (grants 2014SGR97 and XRQTC) and by the NOMAD Center of Excellence project, which received funding from the European Union's Horizon 2020 research and innovation programme under grant agreement No 676580. A. M. G. thanks to Spanish *Ministerio de Economía y Competitividad* for the *Juan de la Cierva* postdoctoral grant (FJCI-2015-23760) and F. I. acknowledges additional support from the 2015 ICREA Academia Award for Excellence in University Research. Computational time at the MareNostrum supercomputer has been provided by the Barcelona Supercomputing Centre through grants from *Red Española de Supercomputación* and the COMPHOTOCAT project 2014112608 and the EXCIPHOCAT project 2016163940 of the Partnership for Advanced Computing in Europe (PRACE).

Table 1. Vertical energy (E_v), relaxation energy (E_{rel}), oxygen vacancy formation energy (E_f^O) and energy level of oxygen vacancy defect state below LUMO (S_v-1 and S_v-2) as predicted from DFT based calculations with the PBEx hybrid functional. All values are in eV units and the lowest E_f^O values are highlighted in bold type. "CN" is number of first neighbor titanium atoms to remove oxygen atom and "site" is the combination of position and CN number.

Position	**CN**	**Site**	$\boldsymbol{E_v}$	$\boldsymbol{E_{rel}}$	$\boldsymbol{E_f^O}$	**S_v-1**	**S_v-2**
Tip	1	T-1	4.48	0.89	3.58	0.64	0.49
Edge	2	E-2	4.71	0.70	4.01	1.68	0.53
Facet	2	F-2	5.26	1.31	3.95	1.15	0.69
	3	F-3	5.02	0.75	4.27	0.56	0.53
Inside	3	I-3-1	4.73	0.69	4.03	1.63	-
	3	I-3-2	4.29	0.72	3.56	0.37	-

Table 2. Vertical energy (E_v), relaxation energy (E_{rel}), oxygen vacancy formation energy (E_f^O) and energy level of oxygen vacancy defect state below LUMO (S_v-1 and S_v-2) as predicted from DFT based calculations with the PBE0 hybrid functional. All values are in eV units and the lowest E_f^O values are highlighted in bold type. "CN" is number of first neighbor titanium atoms to removed oxygen atom and "site" is the combination of position and CN number.

Position	**CN**	**Site**	E_v	E_{rel}	E_f^O	**S_v-1**	**S_v-2**
Tip	1	T-1	4.35	2.86	1.48	0.51	0.28
Edge	2	E-2	4.87	2.88	1.99	2.94	2.43
Facet	2	F-2	5.27	3.34	1.92	2.69	2.21
	3	F-3	5.72	2.93	2.78	1.88	1.70
Inside	3	I-3-1	4.73	2.44	2.28	2.60	-
	3	I-3-2	4.99	2.80	2.19	1.74	1.57

Figure 1. (a) Side and top views of the pristine $(TiO_2)_{84}$ NP. (b) Side and top views of the different reduced $Ti_{84}O_{167}$ NPs. Blue, red and black spheres denote titanium, oxygen and first neighbor titanium atoms to the O_v site, respectively. Note that the reduced NP labeled as I-3-2 is slightly tilted to show clearly the region of O_v site in the subsurface.

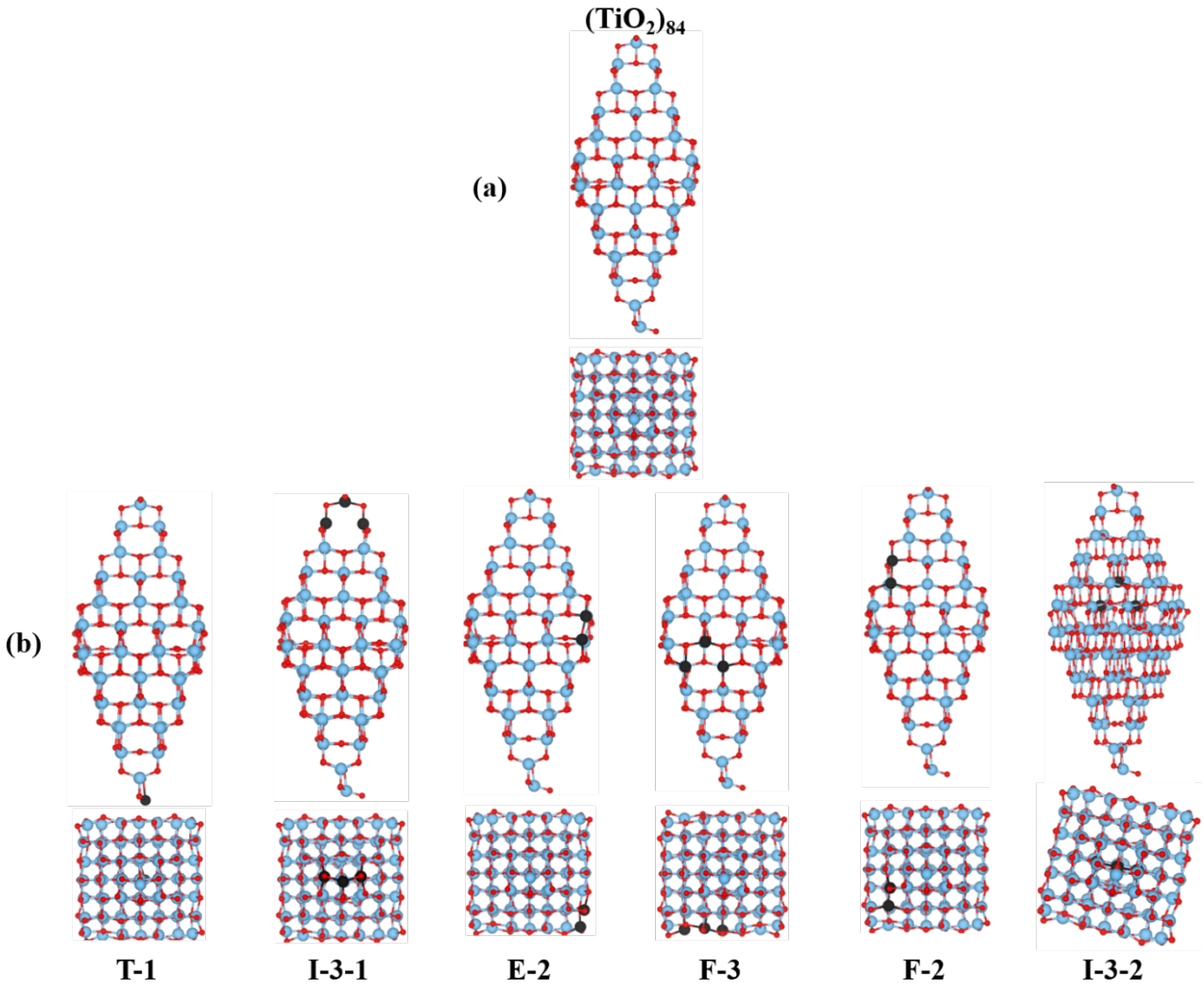

Figure 2. Oxygen vacancy formation energy (E_f^O) for single oxygen vacant $Ti_{84}O_{167}$ nanoparticle at PBE, PBEx and PBE0 levels depicted with black, red and blue navy colors, respectively. Note that dashed gray line indicates that the oxygen vacancy in I-3-2 site is the most favorable domain to create the oxygen vacancy at PBEx level. E_f^O values for PBE, PBEx and PBE0 functionals are compiled in Tables S1, 1 and 2, respectively.

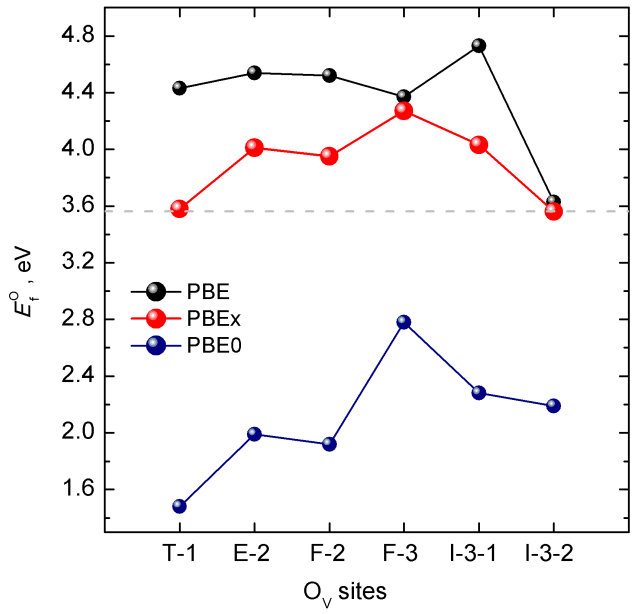

Figure 3. Stoichiometric and reduced $(TiO_2)_{84}$ NP motifs that correspond to the first neighbor titanium atoms to the O_v site depicted in black at Figure 1: (a) T-1 and I-3-1, (b) E-2, (c) F-3, (d) F-2 and (e) I-3-2 and calculated at PBEx level. Blue and red spheres denote titanium and oxygen atoms, respectively.

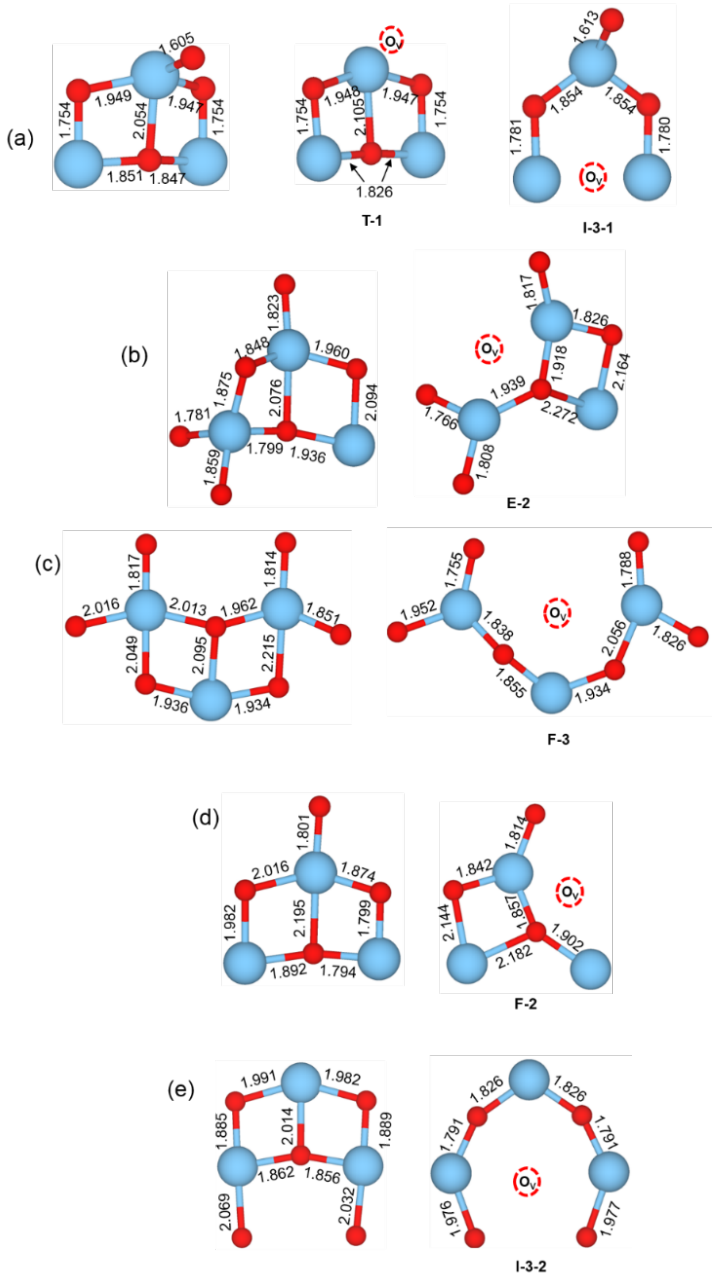

Figure 4. Kohn-Sham orbital energy level diagram of $Ti_{84}O_{168}$ and reduced $Ti_{84}O_{167}$ NPs at obtained from calculations with the PBEx functional. The triplet state energy levels are for spin-up eigenvalues. The red dotted lines correspond to the standard redox potentials for water splitting at pH = 0 (H^+/H_2 = -4.44 eV and O_2/H_2O = -5.67 eV). The singly and doubly occupied defect states are denoted in blue and green for triplet and singlet states, respectively. Other occupied and unoccupied molecular orbitals are represented with black lines.

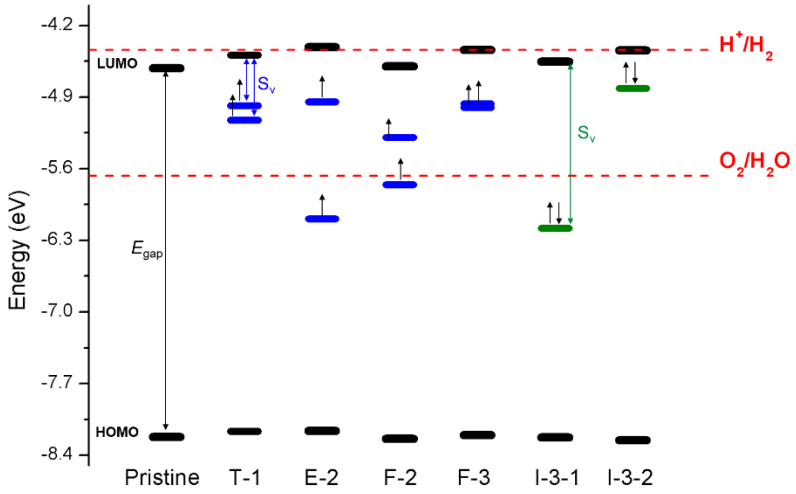

Figure 5. Kohn-Sham orbital energy level diagram of $Ti_{84}O_{168}$ and reduced $Ti_{84}O_{167}$ NPs at PBE0 level. The triplet state energy levels are for spin-up eigenvalues. The red dotted lines correspond to the standard redox potentials for water splitting at pH = 0 (H^+/H_2 = -4.44 eV and O_2/H_2O = -5.67 eV). The singly and doubly occupied defect states are denoted in blue and green for triplet and singlet states, respectively. Other occupied and unoccupied molecular orbitals are represented with black lines.

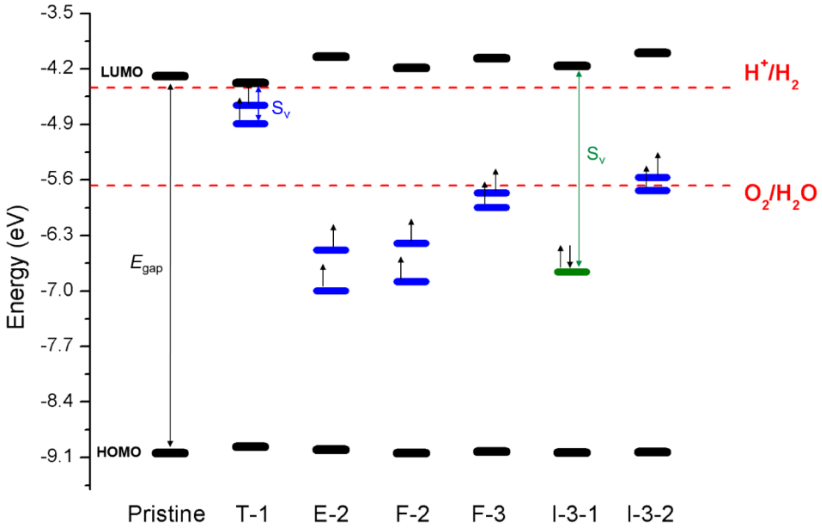

References

1 Fox, M. A.; Dulay, M. T. Heterogeneous photocatalysis. *Chem. Rev.* **1993**, *93*, 341-357.

2 Xu, H.; Ouyang, S.; Liu, L.; Reunchan, P.; Umezawa, N.; Ye, J. Recent advances in TiO_2-based photocatalysis. *J. Mater. Chem. A* **2014**, *2*, 12642-12661.

3 Hashimoto, K.; Irie, H.; Fujishima, A. TiO_2 photocatalysis: a historical overview and future prospects. *Jpn. J. Appl. Phys.* **2005**, *44*, 8269-8285.

4 Fujishima, A.; Zhang, X.; Tryk, D. A. TiO_2 photocatalysis and related surface phenomena. *Surf. Sci. Rep.* **2008**, *63*, 515-582.

5 Maeda, K. Direct splitting of pure water into hydrogen and oxygen using rutile titania powder as a photocatalyst. *Chem. Commun.* **2013**, *49*, 8404-8406.

6 Maeda, K. Photocatalytic properties of rutile TiO_2 powder for overall water splitting. *Catal. Sci. Technol.* **2014**, *4*, 1949-1953.

7 Tang, J.; Durrant, J. R.; Klung, D. R. Mechanism of photocatalytic water splitting in TiO_2. Reaction of water with photoholes, importance of charge carrier dynamics, and evidence for four-hole chemistry. *J. Am. Chem. Soc.* **2008**, *130*, 13885-13891.

8 Banno, H.; Kariya, B.; Isu, N.; Ogawa, M.; Miwa, S.; Sawada, K.; Tsuge, J.; Imaizumi, S.; Kato, H.; Tokutake, K.; Deguchi, S. Effect of TiO_2 crystalline diameter on photocatalytic water splitting rate. *Green Sustainable Chem.* **2014**, *4*, 87-94.

9 Davis, S. J.; Caldeira, K. Consumption-based accounting of CO_2 emissions. *Proc. Natl. Acad. Sci. USA* **2010**, *107*, 5687-5692.

10 Dodman, D. Blaming cities for climate change? An analysis of urban greenhouse gas emissions inventories. *Environ. Urban.* **2009**, *21*, 185-201.

11 Wang, W. N.; An, W. K.; Ramalingam, B.; Mukherjee, S.; Niedzwiedzki, D. M.; Gangopadhyay, S.; Biswas, P. Size and structure matter: enhanced CO_2 photoreduction efficiency by size-resolved ultrafine Pt nanoparticles on TiO_2 single crystals. *J. Am. Chem. Soc.* **2012**, *134*, 11276-11281.

12 Asahi, R.; Morikawa, T.; Irie, H.; Ohwaki, T. Nitrogen-doped titanium dioxide as visible-light-sensitive photocatalyst: designs, developments, and Prospects. *Chem. Rev.* **2014**, *114*, 9824-9852.

13 Liang, Y. T.; Vijayan, B. K.; Gray, K. A.; Hersam, M. C. Minimizing graphene defects enhances titania nanocomposite-based photocatalytic reduction of CO_2 for improved solar fuel production. *Nano Lett.* **2011**, *11*, 2865-2870.

[14] Wang, C.; Thompson, R. L.; Baltrust, J.; Matranga, C. Visible light photoreduction of CO_2 using CdSe/Pt/TiO_2 heterostructured catalysts. *J. Phys. Chem. Lett.* **2010**, *1*, 48-53.

[15] Liu, G.; Yang, H. G.; Pan, J.; Yang, Y. Q.; Lu, G. Q.; Cheng, H. M. Titanium dioxide crystals with tailored facets. *Chem. Rev.* **2014**, *114*, 9559-9612.

[16] Wang, X.; Li, Z.; Shi, J.; Yu, Y. One-dimensional titanium dioxide nanomaterials: nanowires, nanorods, and nanobelts. *Chem. Rev.* **2014**, *114*, 9346-9384.

[17] Pan, X.; Yang, M. Q.; Fu, X.; Zhang, N.; Xu, Y. J. Defective TiO_2 with oxygen vacancies: synthesis, properties and photocatalytic applications. *Nanoscale* **2013**, *5*, 3601-3614.

[18] Naldoni, A.; Allieta, M.; Santangelo, S.; Marelli, M.; Fabbri, F.; Cappelli, S.; Bianchi, C. L.; Psaro, R.; Dal Santo, V. Effect of nature and location of defects on bandgap narrowing in black TiO_2 nanoparticles. *J. Am. Chem. Soc.* **2012**, *134*, 7600-7603

[19] Sekiya, T.; Yagisawa, T.; Kamiya, N.; Das Mulmi, D.; Kurita, S.; Murakami, Y.; Kodaira, T. Defects in anatase TiO_2 single crystal controlled by heat treatments. *J. Phys. Soc. Jpn.* **2004**, *73*, 703-710.

[20] Amano, F.; Nakata, M.; Yamamoto, A.; Tanaka, T. Effect of Ti^{3+} ions and conduction band electrons on photocatalytic and photolectrochemical activity of rutile titania for water oxidation. *J. Phys. Chem. C* **2016**, *120*, 6467-6474.

[21] Qiu, M.; Tian, Y.; Chen, Z.; Yang, Z.; Li, W.; Wang, K.; Wang, L.; Wang, K.; Zhang W. Synthesis of Ti^{3+} self-doped TiO_2 nanocrystals based on Le Chatelier´s principle and their application in solar light photocatalysis. *RSC Adv.* **2016**, *6*, 74376-74383.

[22] Liu, L.; Jiang, Y.; Zhao, H.; Chen, J.; Cheng, J.; Yang, K.; Li, Y. Engineering coexposed {001} and {101} facets in oxygen-deficient TiO_2 nanocrystals for enhanced CO_2 photoreduction under visible light. *ACS Catal.* **2016**, *6*, 1097-1108.

[23] Ko, K. C.; Lamiel-García, O.; Lee, J. Y.; Illas, F. Performance of a modified hybrid functional in the simultaneous description of stoichiometric and reduced TiO_2 polymorphs. *Phys. Chem. Chem. Phys.* **2016**, *18*, 12357−12367.

[24] Wang, M.; Feng, M.; Lu, Y. Ab initio study of the anion vacancy on anatase TiO_2 (101) surface. *Mod. Phys. Lett. B* **2014**, *28*, 1450076 (1-8).

[25] Li, H.; Guo, Y.; Robertson, J. Calculation of TiO_2 surface and subsurface oxygen vacancy by the screened exchange functional. *J. Chem. Phys. C* **2015**, *119*, 18160-18166.

[26] Kim, S.; Ko, K. C.; Lee, J. Y.; Illas, F. Single oxygen vacancies of $(TiO_2)_{35}$ as a prototype reduced nanoparticle: implication for photocatalytic activity. *Phys. Chem. Chem. Phys.* **2016**, *18*, 23755-23762.

[27] Lamiel-García, O.; Cuko, A.; Calatayud, M.; Illas, F.; Bromley, S. T. Predicting size-dependent emergence of crystallinity in nanomaterials: titania nanoclusters versus nanocrystals. *Nanoscale* **2017**, *9*, 1049-1058.

[28] Liu, G.; Yang, H. G.; Pan, J.; Yang, Y. Q.; Lu, G. Q. M.; Cheng, H. M. Titanium dioxide crystals with tailored facets. *Chem. Rev.* **2014**, *114*, 9559−9612.

[29] Cho, D.; Ko, K. C.; Lamiel-García, O.; Bromley, S. T.; Lee, J. Y. Effect of size and structure on the ground-state and excited-state electronic structure of TiO_2 nanoparticles. *J. Chem. Theory Comput.* **2016**, *12*, 3751-3763.

[30] Lamiel-García, O.; Ko, K. C.; Lee, J. Y.; Bromley, S. T.; Illas, F. When anatase nanoparticles become bulklike: Properties of realistic TiO_2 nanoparticles in the 1−6 nm size range from all electron relativistic density functional theory based calculations. *J. Chem. Theory Comput.* **2017**, *13*, 1785−1793.

[31] Morales-García, A.; Valero, R.; Illas, F. Performance of the G_0W_0 method in predicting the electronic gap of TiO_2 nanoparticles. *J. Chem. Theory Comput.* **2017**, *13*, 3746-3753.

[32] Almquist, C. B.; Biswas, P. Role of synthesis method and particle size of nanostructured TiO_2 on its photoactivity. *J. Catal.* **2002**, *212*, 145-156.

[33] Cococcioni, M.; de Gironcoli, S. Linear response approach to the calculation of the effective interaction parameters in the LDA+U method. *Phys. Rev. B* **2005**, *71*, 035105 (1-16).

[34] Mori-Sánchez, P.; Cohen, A. J.; Yang, W. Localization and delocalization errors in density functional theory and implications for band-gap prediction. *Phys. Rev. Lett.* **2008**, *100*, 146401 (1-4).

[35] Adamo, C; Barone, V. Toward reliable density functional methods without adjustable parameters: The PBE0 model. *J. Chem. Phys.* **1999**, *110*, 6158-6169

[36] Perdew, J. P.; Burke, K.; Ernzerhof, M. Generalized gradient approximation made simple. *Phys. Rev. Lett.* **1996**, *77*, 3865−3868

[37] Deringer, V.L.; Csányi, G. Many-Body Dispersion Correction Effects on Bulk and Surface Properties of Rutile and Anatase TiO_2. *J. Phys. Chem. C* **2016**, *120*, 21552-21560

[38] Blum, V.; Gehrke, R.; Hanke, P.; Havu, P.; Havu, V.; Ren, X.; Reuter, K.; Scheffler, M. Ab initio molecular simulations with numeric atom-centered orbitals. *Comput. Phys. Commun.* **2009**, *180*, 2175-2196.

[39] Chang, C., Pelissier, M.; Durand, M. Regular two-component Pauli-like effective hamiltonians in Dirac theory. *Phys. Scr.* **1986**, *34*, 394-404

[40] van Lenthe, E.; van Leeuwen, R.; Baerends E. J.; Snijders J. G. Relativistic regular two-component hamiltonians *Int. J. Quantum Chem.* **1994**, *57*, 281-293.

[41] Wulff, G. On the question of speed of growth and dissolution of crystal surfaces. *Z. Kristallogr.* **1901**, *34*, 449−530.

[42] Bromley, S. T.; Moreira, I. De P.R.; Neyman, K.-M.; Illas, F. Approaching nanoscale oxides: models and theoretical methods. *Chem. Soc. Rev.* **2009**, *38*, 2657−2670.

[43] Lazzeri, M.; Vittadini, A.; Selloni, A. Structure and energetics of stoichiometric TiO_2 anatase surfaces. *Phys. Rev. B: Condens. Matter Mater. Phys.* **2001**, *63*, 155409.

[44] Kavan, L.; Grätzel, M.; Gilbert, S. E.; Klemenz, C.; Scheel, H. J. Electrochemical and photoelectrochemical investigation of single-crystal anatase. *J. Am. Chem. Soc.* **1996**, *118*, 6716-6723.

[45] He, Y.; Dulub, O.; Cheng, H.; Selloni, A.; Diebold U. Evidence for the predominance of subsurface defect on reduced anatase TiO_2 (101). *Phys. Rev. Lett.* **2009**, *102*, 106105 (1-4).

[46] Scheiber, P.; Fidler, M.; Dulub, O.; Schmid, M.; Diebold, U.; Hou, W.; Aschauer, U.; Selloni, A. (Sub)Surface mobility of oxygen vacancies at the TiO_2 anatase (101) surface. *Phys. Rev. Lett.* **2012**, *109*, 136103 (1-5).

[47] Finazzi, E.; Di Valentin, C.; Pacchioni, G.; Selloni, A. Excess electron states in reduced bulk anatase TiO_2: Comparison, of standard GGA, GGA+*U*, and hybrid DFT calculations. *J. Chem. Phys.* **2008**, *129*, 154113 (1-9).

[48] Ni, M.; Leung, M. K. H.; Leung, D. Y. C.; Sumathy, K. A review and recent developments in photocatalytic water-splitting using TiO_2 for hydrogen production. *Renewable Sustainable Energy Rev.* **2007**, *11*, 401-425.

[49] Migani, A.; Vayssilov, G. N.; Bromley, S. T.; Illas, F.; Neyman, K. M. Greatly facilitated oxygen vacancy formation in ceria crystallites at nanoscale. *Chem. Commun.* **2010**, 5936-5938

[50] Migani, A.; Vayssilov, G. N.; Bromley, S. T.; Illas, F.; Neyman, K. M. Dramatic reduction of the oxygen vacancy formation energy in ceria particles: A possible key to their remarkable reactivity at the nanoscale. *J. Mater. Chem.,* **2010**, *20*, 10535-10546

[51] Low, J.; Jiang, C.; Cheng, B.; Wageh, S.; Al-Ghamdi, A. A.; Yu. J. A review of direct Z-scheme photocatalysts. *Small Methods* **2017**, *1*, 1700080 (1-21).

TOC Graphics